Adaptive PPF Control Using a Modified EKF Observer

M.Sc. thesis

Kosar Gharajehdaghi

Committee:

Prof.dr.ir. W.B.J. Hakvoort
Prof.dr.ir G.J.M. Krijnen
Ir. B. Seinhorst

Date: 28/03/2025

Control and Mechatronics,
Faculty of Engineering Technology
University of Twente,
The Netherlands

Contents

Abstract

This thesis presents an approach for suppressing parasitic vibrations in flexure-based structures with varying resonance frequencies by integrating an indirect adaptive Positive Position Feedback controller with an Extended Kalman Filter estimator. Flexure-based systems experience changes in resonance frequency due to elasto-kinematic effects, which require real-time adaptation of the PPF controller parameters to maintain optimal performance.

The focus of this study is on the low-frequency vibration mode, therefore a reduced single-degree-of-freedom model is used to represent the system, specifically a cantilever beam. However, to account for the effects of higher resonance modes on the first vibration mode, a direct feed-through term is added to the system model.

An EKF algorithm is developed to estimate the system's resonance frequency by treating stiffness as an additional state variable. The estimated resonance frequency is used to adaptively update the PPF controller parameters, improving vibration suppression, and maintaining robustness.

The presence of the direct feed-through term in the system model equations leads to unconventional correlations in the EKF formulation. Therefore, the EKF algorithm is re derived to account for these correlations.

Finally, the proposed method is validated through numerical simulations, demonstrating its ability to maintain system stability and effectively suppress parasitic vibrations compared to traditional PPF controllers with fixed parameters.

1 Introduction

1.1 Background

Precision machines are designed to achieve high performance by maintaining both accuracy and speed. Therefore it is needed to omit any kinds of inaccuracies from the design of the plant. Conventional mechanisms often exhibit friction and hysteresis effects, introducing uncertainties into the system and making precise positioning challenging [1].

Flexure mechanisms can potentially overcome these challenges. These structures are characterized by low friction, lightweight construction, and high stiffness in their support direction, also known as the degree of constraint [2]. These qualities ensure that the parasitic resonance frequencies are as high as possible. However, flexure mechanisms also present certain difficulties. While they exhibit significant stiffness in their support direction, this stiffness is not infinite and tends to decrease under large deflections. Additionally, their inherently low damping contributes to the emergence of problematic parasitic resonance frequencies at lower values, which can degrade the control bandwidth and, consequently, the positioning accuracy of the system.

As further improvements in flexure design become increasingly challenging [3], alternative solutions are being explored. One such approach involves suppressing parasitic resonance frequencies by incorporating a damping element into the system.

Traditional passive vibration suppression methods, such as incorporating tuned mass dampers or viscoelastic materials, aim to mitigate these resonance vibrations, come with different pros and cons. For instance, while they are very reliable and robust, they may interfere with the design of the flexures, adding unwanted complexities to the plant [4].

Alternatively, active vibration suppression methods have gained significant attention. These approaches typically involve structures embedded with active materials, particularly piezoelectric materials, for vibration suppression. Due to their atomic lattice structure, piezoelectric materials enable the use of piezoelectric sensors and actuators, which convert mechanical deformation (strain) into electrical signals and vice versa at a small scale. Notably, piezoelectric patches offer the advantage of preserving mechanical design simplicity without adding extra mass, thereby enabling effective resonance suppression even at higher frequencies [5].

1.2 Literature Review

In recent years, various control methods have been employed to suppress vibrations, including velocity feedback, resonant controllers, and positive position feedback (PPF). These approaches fall under collocated control techniques, where sensors and actuators are associated with the same degree of freedom (DOF) of the structure. A key advantage of collocated systems is their inherent closed-loop stability concerning out-of-bandwidth dynamics [6].

In a velocity feedback controller [7], a positive gain is chosen to enhance damping, leading to high control effort across all frequencies and eliminating roll-off at high frequencies. Despite ensuring closed-loop stability, this approach can introduce spillover issues. Additionally, since piezoelectric sensors measure strain, a differentiator is required to obtain velocity from position, which is generally undesirable as it amplifies noise.

The resonant controller operates as a second-order high-pass filter with negative feedback. Similar to the velocity feedback controller, it does not exhibit roll-off at high frequencies and is susceptible to spillover effects (A more detailed definition will be given later).

The PPF controller, first proposed by Goh and Caughey in 1985 [8], is another widely used control strategy for active vibration control. PPF operates as a second-order low-pass filter that quickly rolls off at high frequencies, thus limiting high-frequency spillover; however, it does not prevent low-frequency spillover, which causes changes both in magnitude and frequency of lower vibration modes in the closed-loop response [9].

The effectiveness of both PPF and resonant controllers depends heavily on the proper tuning of their parameters, which are directly influenced by the system's resonance frequency. Therefore, prior knowledge of the resonance frequency is expected to enhance controller performance. However, as demonstrated in [10], the resonance frequency of flexure mechanisms may vary significantly with large deflections. This variation reduces the robustness of the PPF controller and diminishes its effectiveness in vibration suppression.

In recent years, several studies have focused on reducing vibrations in dynamic systems through the development of adaptive controllers that adjust to changes in resonance frequency by tracking and estimating these frequencies. These studies employ various controller methodologies in conjunction with diverse frequency estimation algorithms.

One widely adopted method for harmonic detection is the Fast Fourier Transform (FFT), which has been utilized extensively for frequency estimation. For instance, a real-time identification study using the Sliding Discrete Fourier Transform (SDFT) is conducted in [11]. Their findings demonstrate that this approach can effectively obtain real-time frequency response estimates using limited data within a sliding window. Experimental results further validate that the SDFT method successfully tracks and updates changes within the system. Similarly, Kang et.al [12] employed the SDFT technique for the online estimation of mechanical resonances, utilizing this information to adjust the parameters of a notch filter aimed at suppressing resonance effects. Mahmoodi et al. [13] developed an adaptive modified PPF, which comprises two components: the first focuses on frequency adaptation through FFT estimation, while the second integrates this information into the Modified PPF. Although this frequency adaptation method has been experimentally validated, it is limited by the constraints of the FFT, particularly its need for substantial data storage before it can operate effectively. Therefore, alternative frequency estimation techniques should also be considered to improve speed.

The inventor of PPF control [14] proposed an adaptive identification approach utilizing a persistently excited input signal.

Another notable approach for frequency estimation is the Extended Kalman Filter (EKF), which has been the focus of considerable research, including contributions from La Scala and Bitmead [15].

Moreover, significant advancements have been made in adaptive active vibration control, with many studies concentrating on the design parameters of the PPF controller. Some researchers use H_2 and H_∞ minimization techniques to synthesize optimal PPF controllers [16], while others estimate PPF parameters through real-time adaptive methods [13], [9].

The research gap identified is the inadequate performance of the Fast Fourier Transform (FFT) in the work of Mahmoodi et al. [13], particularly regarding rapidly varying resonance frequencies of a flexure beam. To address this, we propose replacing FFT with faster estimation algorithms, such as the Extended Kalman Filter, which has demonstrated superior performance in several studies, including those by La Scala and Bitmead [15].

The idea of using an adaptive active vibration control to enhance the performance of the resonance suppression has been considered before. One example is paper [17] where an adaptive resonance controller has been designed with on-line resonance frequency estimator to update the resonant controller parameters.

2 Modeling and Controller Method

2.1 Introduction

Developing a comprehensive mathematical model of a system is essential for analyzing a plant, designing a controller, and simulating the effects of any modifications. The first subsection 2.2 in this chapter is allocated to this matter. We know that flexible structures, in general, inherently possess infinite vibration modes and can be accurately represented using high-order transfer functions. While such models are most useful for accurate simulations, in order to facilitate control design, a reduced-order model of the actual plant comes in handy. This simplification, however, comes at a cost, as high-frequency dynamics omitted from the model may impact system stability. The Positive Position Feedback controller is expected to address this issue due to its second-order roll-off at high frequencies. Subsection 2.3, explains this control technique and how tuning its parameters can give optimal performance.

2.2 Mathematical Modeling

The plant that is considered for this study is a cantilever beam. It has the same characteristics as the one introduced in [16]. Figure 1 illustrates a schematics of the beam. The beam is supposed to be excited by an external disturbance (w) originating from the ground. The vibrations of the tip of the beam are intended to be suppressed. For this purpose, a capacitive sensor is used there to measure these vibrations. As mentioned before, an active vibration control using piezo-electric patches is meant to be used for resonance suppression. Two piezo patches are mounted on the beam in a collocated configuration, one functioning as a sensor to measure strain and the other as an actuator to apply control input. The placement of piezo patches is chosen considering where there is the most strain in the system at the first vibration mode.

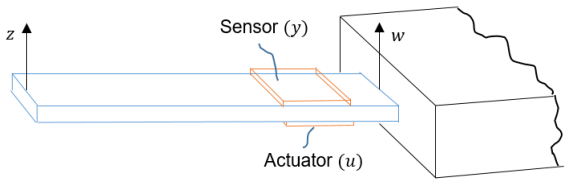

Figure 1: Schematic representation of the cantilever beam.

As previously mentioned, flexible structures exhibit an infinite number of vibration modes. However, this study focuses on suppressing the system's low-frequency resonance. Therefore, the system can be approximated as a Single Degree of Freedom (SDOF) oscillator, governed by the following mathematical model:

$$m\ddot{x} + c\dot{x} + kx = B_u u + B_d w_d, \tag{1}$$

$$\begin{bmatrix} z \\ y \end{bmatrix} = \begin{bmatrix} f_z \\ f_y \end{bmatrix} x + \begin{bmatrix} d_{zw} & d_{zu} \\ d_{yw} & d_{yu} \end{bmatrix} \begin{bmatrix} w_d \\ u \end{bmatrix}, \tag{2}$$

where,

$$x : \text{Generalized coordinate},$$
$$m : \text{Equivalent mass},$$
$$k : \text{Equivalent stiffness},$$
$$c : \text{Equivalent internal damping},$$
$$\begin{bmatrix} B_d & B_u \end{bmatrix} : \text{Input matrix},$$
$$\begin{bmatrix} f_z \\ f_y \end{bmatrix} : \text{Output matrix},$$
$$\begin{bmatrix} d_{zw} & d_{zu} \\ d_{yw} & d_{yu} \end{bmatrix} : \text{Feedthrough matrix}.$$

The feed-through term is introduced in the mathematical equations of the SDOF mass-spring-damper system to account for higher-frequency effects. An experiment conducted in [16] demonstrates that the system's frequency response may lack roll-off at high frequencies, which is for example typical for systems with collocated sensing and actuation. As shown in Figure 2, the absence of roll-off in the experimental frequency response highlights the need for a feed-through term. By incorporating this term, the model captures the low-frequency effects of higher resonances, leading to a more accurate fit for the resonance to be suppressed.

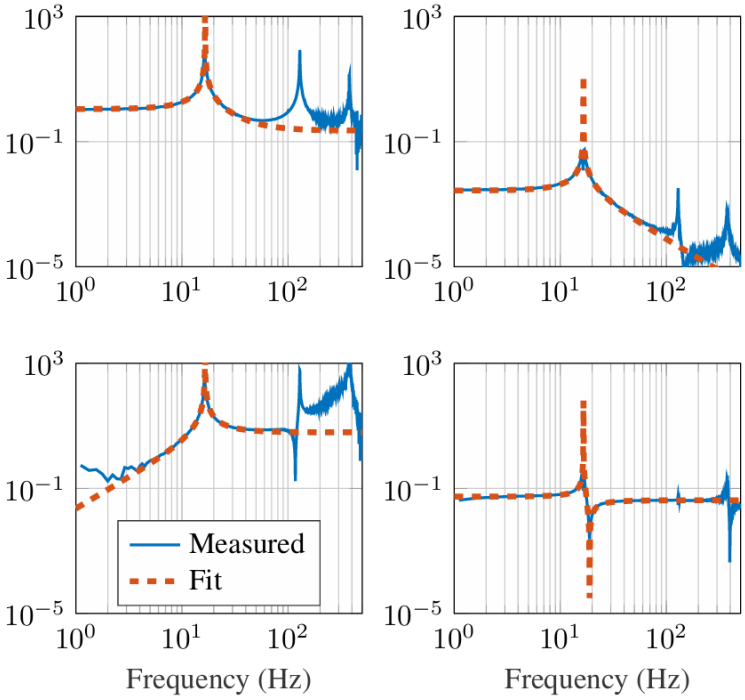

Figure 2: The bode plots of transfer functions, in order from top left, T_{zw}, top right T_{zu}, bottom left T_{yw}, and bottom right T_{yu}. (This Figure is borrowed from the reference [16])

Using the low and high frequency asymptotes of the reduced plant, system parameters, γ_{yu}, γ_{yw}, γ_{zu}, and γ_{zw} can be calculated [16]. To show this, equations (1) and (2) are converted to Laplace

domain, where the transfer functions T_{zw}, T_{zu}, T_{yw}, and T_{yu} are derived as follows:

$$
\begin{aligned}
T_{yu} &= \frac{f_y b_u}{s^2 + \frac{c}{m}s + \omega_n^2} + d_{yu}, \\
T_{yw} &= \frac{f_y b_d}{s^2 + \frac{c}{m}s + \omega_n^2} + d_{yw}, \\
T_{zu} &= \frac{f_z b_u}{s^2 + \frac{c}{m}s + \omega_n^2} + d_{zu}, \\
T_{zw} &= \frac{f_z b_d}{s^2 + \frac{c}{m}s + \omega_n^2} + d_{zw},
\end{aligned}
$$

where,

$$
b_u = \frac{B_u}{m}, b_d = \frac{B_d}{m}.
$$

Now as defined in [4], γ parameters can be expressed as:

$$
\gamma_{ij} = \frac{P_{ij}|_{\omega=\infty}}{P_{ij}|_{\omega=0} - P_{ij}|_{\omega=\infty}}, \tag{3}
$$

where the asymptotes of the reduced plant at low and high frequencies can be obtained as:

$$
\begin{aligned}
P_{ij}|_{\omega=0} &= \begin{bmatrix} \frac{f_y b_u}{\omega_n^2} & \frac{f_y b_d}{\omega_n^2} \\ \frac{f_z b_u}{\omega_n^2} & \frac{f_z b_d}{\omega_n^2} \end{bmatrix} + \begin{bmatrix} d_{yu} & d_{yw} \\ d_{zu} & d_{zw} \end{bmatrix}, \\
P_{ij}|_{\omega=\infty} &= \begin{bmatrix} d_{yu} & d_{yw} \\ d_{zu} & d_{zw} \end{bmatrix}.
\end{aligned} \tag{4}
$$

Plugging in equation (4) in (3) results in:

$$
\begin{bmatrix} \gamma_{yu} & \gamma_{yw} \\ \gamma_{zu} & \gamma_{zw} \end{bmatrix} = \omega_n^2 \begin{bmatrix} \frac{d_{yu}}{f_y b_u} & \frac{d_{yw}}{f_y b_d} \\ \frac{d_{zu}}{f_z b_u} & \frac{d_{zw}}{f_z b_d} \end{bmatrix}. \tag{5}
$$

The γ parameter values are calculated for this plant in [16], so assuming the input and output matrix are known, the feed-through matrix can be calculated.

2.3 Positive Position Feedback Control and H_2 Optimization

Positive Position Feedback (PPF) control is an effective strategy for vibration suppression in structures with collocated actuator-sensor configurations. As observed in Figure 2, the T_{yu} transfer function lacks the expected high-frequency roll-off. This characteristic indicates that other collocated control techniques discussed in the introduction may not be suitable for this system. While these methods theoretically ensure closed-loop stability with appropriately chosen controller gains, in practice, even a slight misalignment in the placement of the piezoelectric sensor and actuators can destabilize the system due to the spillover effect.

Spillover typically occurs when the high-frequency resonances of a system, which have been truncated in a reduced-order model, are inadvertently amplified by the controller. This amplification arises when the controller distributes actuation energy across all system frequencies, as seen in velocity feedback control, or selectively excites high-frequency resonances, as in resonant control. Consequently, this phenomenon can potentially destabilize the system.

On the other hand, the PPF controller operates as a second-order low-pass filter, which helps mitigate the spillover effect due to its roll-off at high frequencies.

PPF control positively feeds the position measurement into the compensator, and the compensator's output is then positively fed back into the structure. This intrinsic characteristic makes PPF control

particularly well-suited for piezoelectric sensors, which both measure and impose displacement on the structure.

The PPF controller can be expressed in the form of:

$$\begin{aligned} \ddot{q} + 2\zeta_c \omega_c \dot{q} + \omega_c^2 q &= k_s \omega_c y \\ u &= k_a \omega_c q, \end{aligned} \tag{6}$$

where, w_c is the controller resonance frequency, ζ_c is the controller damping ratio, and the low frequency gain of the system is defined as $k = k_s k_a > 0$ where k_s corresponds to sensing gain and k_a for actuation gain specifically.

Tuning the parameters of the PPF controller is essential to achieve the desired performance in resonance suppression with an acceptable stability margin. An experimental robustness study of PPF control for active vibration suppression of a smart flexible structure is done in [18]. It concludes that increasing ζ_c improves robustness while slightly reducing the effectiveness at the target frequency. The findings suggest using a higher ζ for robustness, around 0.5 for practical implementation. An analytical solution to the PPF parameter tuning based on gain margin constrained H_2 optimization is provided in [16]. The minimization problem is defined as:

$$\arg \min_{k,\omega_c,\zeta_c} \|G(s)\|, \tag{7}$$

where $G(s)$ indicates the closed-loop system from w to z. Finally, the resulted optimally tuned controller parameters are obtained as given in the following equations:

$$k = \frac{g}{1+\gamma_{yu}} \frac{\omega_n^2}{f_y b_u}, \tag{8}$$

$$\frac{\omega_c}{\omega_n} = \frac{1}{\sqrt{1 - g\frac{\gamma_{yu} - \gamma_{yw} - \gamma_{zu}}{1+\gamma_{yu}}}}, \tag{9}$$

$$\zeta_c = \frac{1}{2}\sqrt{\frac{g}{1-g}} \frac{1 - g\frac{\gamma_{yu} - \gamma_{yw} - \gamma_{zu} - \gamma_{yw}\gamma_{zu}}{1+\gamma_{yu}}}{\sqrt{1+\gamma_{yu}}\sqrt{1 - g\frac{\gamma_{yu} - \gamma_{yw} - \gamma_{zu}}{1+\gamma_{yu}}}}, \tag{10}$$

where the static open loop gain, denoted as g will be defined in next chapter.

As seen in equations (8), (9), and (10), the optimally tuned PPF parameters are highly dependent on the system's resonance frequency,ω_n. In applications where the targeted resonance frequency varies significantly [10], it becomes crucial to estimate it with sufficient accuracy. Accurate estimation allows for the selection of smaller values for ζ_c, leading to improved damping performance while ensuring that system robustness is not compromised.

3 PPF Adaptation

3.1 Introduction

Effective vibration system control usually requires identifying the dominant vibration modes, especially when the system deviates from its nominal model during operation. These deviations can result from factors such as varying payloads, additional mounted sensors and actuators, the change of capacitance in piezo sensors due to humidity, or mechanical fatigue over time [14]. In this study, modeling uncertainties are constrained to a single varying parameter: the structure's stiffness. This chapter presents a modified Extended Kalman Filter based observer for efficiently estimating the system's varying stiffness due to elasto-kinematic effects [19], in real time, enabling a rapid adaptation of the optimized PPF controller for resonance suppression performance.

3.2 Kalman Filtering and Parameter Estimation

In 1960, Rudolf E. Kálmán [20] introduced a mathematical technique for state estimation in linear dynamic systems subject to noisy measurements and system uncertainties, now known as the Kalman Filter (KF). The KF models the system state as a random variable affected by Gaussian-distributed uncertainties, referred to as process noise. Estimation is performed based on noisy, Gaussian-distributed measurements, known as measurement noise. Using Bayesian inference, the filter employs a recursive algorithm in which the posterior probability of the state is updated at each iteration by combining the likelihood of the new observation with the prior belief derived from the system dynamics.

The KF is recognized as an optimal estimation technique, as it updates the prior state estimate using a correction factor, known as the Kalman gain, which is computed by minimizing the mean square error. Since its inception, the KF has become a fundamental tool in numerous fields, including control systems, robotics [21], and aerospace engineering. In this study, since the objective is to estimate the system's resonance frequency by tracking variations in stiffness, the KF framework is employed for parameter estimation.

The mathematical model of the system, as defined in chapter 2, can be expressed in state-space form as follows:

$$\begin{bmatrix} \dot{x}(t) \\ \ddot{x}(t) \end{bmatrix} = \begin{bmatrix} 0 & 1 \\ -\frac{k(t)}{m} & -\frac{c}{m} \end{bmatrix} \begin{bmatrix} x(t) \\ \dot{x}(t) \end{bmatrix} + \begin{bmatrix} 0 & 0 \\ b_d & b_u \end{bmatrix} \begin{bmatrix} w_d(t) \\ u(t) \end{bmatrix}. \tag{11}$$

The goal is to estimate the system's resonance frequency by determining the stiffness while assuming the mass remains constant throughout the experiment. The resonance frequency can be directly calculated using:

$$\omega_n(t) = \sqrt{\frac{k(t)}{m}}. \tag{12}$$

To achieve this, the state vector is augmented to include the stiffness parameter:

$$\mathbf{x}_{aug}(t) = \begin{bmatrix} x(t) \\ \dot{x}(t) \\ k(t) \end{bmatrix}. \tag{13}$$

By substituting the augmented state vector into the state-space equation, the system model is reformulated to:

$$\frac{d}{dt}\mathbf{x}_{aug}(t) = \begin{bmatrix} \dot{x}(t) \\ -\frac{k(t)}{m}x(t) - \frac{c}{m}\dot{x}(t) + b_u u(t) \\ 0 \end{bmatrix} + \begin{bmatrix} 0 \\ b_d \\ 0 \end{bmatrix} w_d(t) + \begin{bmatrix} 0 \\ 0 \\ 1 \end{bmatrix} w_k(t). \tag{14}$$

It can be observed that the augmented system model becomes nonlinear. Therefore, the Extended Kalman Filter (EKF), which is designed for nonlinear systems, should be employed in this case.

In parameter estimation problems using EKF, it is common to assume that the parameter to be estimated remains constant over time while accounting for its unknown dynamics by introducing a process noise term, denoted as w_k. However, as will be discussed in the next chapter, incorporating prior knowledge of the dynamic behavior of stiffness variations in more complex systems can significantly enhance estimation accuracy.

The state-space equation can be in general written into the following nonlinear form:

$$\dot{\mathbf{x}}_{aug}(t) = f(\mathbf{x}_{aug}(t), u(t)) + Gw(t) \tag{15}$$

where,

$$\begin{aligned} f(\mathbf{x}_{aug}(t), u(t)) &= \begin{bmatrix} \dot{x}(t) \\ -\frac{k(t)}{m}x(t) - \frac{c}{m}\dot{x}(t) + b_u u(t) \\ 0 \end{bmatrix} \\ G &= \begin{bmatrix} 0 & 0 \\ b_d & 0 \\ 0 & 1 \end{bmatrix} \\ w(t) &= \begin{bmatrix} w_d(t) & w_k(t) \end{bmatrix}^T \end{aligned} \tag{16}$$

Similarly, for the output equation, we have:

$$\begin{bmatrix} z(t) \\ y(t) \end{bmatrix} = \begin{bmatrix} f_z & 0 & 0 \\ f_y & 0 & 0 \end{bmatrix} \mathbf{x}_{aug}(t) + \begin{bmatrix} d_{zw}(t) & d_{zu}(t) \\ d_{yw}(t) & d_{yu}(t) \end{bmatrix} \begin{bmatrix} w_d(t) \\ u(t) \end{bmatrix}. \tag{17}$$

Calculating the feed-through matrix using equation (5) results in:

$$\begin{bmatrix} z(t) \\ y(t) \end{bmatrix} = \begin{bmatrix} f_z x(t) + \gamma_{zu}\frac{f_z b_u m}{k(t)}u(t) \\ f_y x(t) + \gamma_{yu}\frac{f_y b_u m}{k(t)}u(t) \end{bmatrix} + \begin{bmatrix} \gamma_{zw}\frac{f_z b_d m}{k(t)} & 0 \\ \gamma_{yw}\frac{f_y b_d m}{k(t)} & 0 \end{bmatrix} w(t). \tag{18}$$

Additionally, the measurement output of the piezoelectric sensor is typically corrupted by a measurement noise, denoted as v(t). Thus, the measurement equation can be expressed in the following general nonlinear form:

$$y(t) = h(\mathbf{x}_{aug}(t), u(t)) + H(t)w(t) + v(t) \tag{19}$$

The term $'H(t)w(t)'$ in the measurement equation (19) introduces a direct correlation between $y(t)$ and $w(t)$, which is not a conventional assumption in EKF. As a result, in the next subsection, modified EKF equations will be rederived accounting for this dependency.

3.2.1 Derivation of the Modified Extended Kalman Filter Equations

First, the system equations (15) and (19) are discretized using the first-order Euler approximation. This step is essential for numerical implementation in computer simulations.

$$\mathbf{x}_{aug}[n+1] = \tilde{f}(\mathbf{x}_{aug}[n], u[n]) + \tilde{G}w[n], \tag{20}$$

$$y[n] = \tilde{h}(\mathbf{x}_{aug}[n]), u[n]) + \tilde{H}[n]w[n] + v[n], \tag{21}$$

where,

$$\begin{aligned} \tilde{f}(\mathbf{x}_{aug}[n], u[n]) &= \mathbf{x}_{aug}[n] + T_s f(\mathbf{x}_{aug}[n], u[n]), \\ \tilde{h}(\mathbf{x}_{aug}[n]), u[n]) &= \mathbf{x}_{aug}[n] + T_s h(\mathbf{x}_{aug}[n]), u[n]), \\ \tilde{G} &= T_s G, \end{aligned}$$

$$\tilde{H}[n] = T_s H[n],$$

and T_s is the sampling time. Kalman Filtering is based on stochastic processes, where state $\mathbf{x}_{aug}$ is considered as a random Gaussian distributed variable with mean and covariance as $(\bar{x}, P_{xx})$. Additionally, process noise, $w[n]$, and measurement noise $v[n]$, are both also assumed as normal distributed zero mean white noises, defined as follows:

$$w[n] \sim \mathcal{N}(0, Q), \tag{22}$$

$$v[n] \sim \mathcal{N}(0, R), \tag{23}$$

where,

$$\begin{aligned} Q &= \mathbb{E}[w[n]w[n]^T] \\ R &= \mathbb{E}[v[n]v[n]^T]. \end{aligned} \tag{24}$$

Moreover, all $w[n]$, $v[n]$ and $\mathbf{x}_{aug}[n]$ are considered to be uncorrelated.

$$\begin{aligned} \mathbb{E}[w[i]v[j]^T] = 0 \quad \text{for all } i \text{ and } j \\ \mathbb{E}[w[i]\mathbf{x}_{aug}[j]^T] = 0 \quad \text{for all } i \text{ and } j \\ \mathbb{E}[v[i]\mathbf{x}_{aug}[j]^T] = 0 \quad \text{for all } i \text{ and } j \end{aligned} \tag{25}$$

For simplicity, the derivation is carried out by representing the augmented state, $\mathbf{x}_{aug}$, as x. It is important to note that, since no standard Kalman Filter algorithm was found for a system exhibiting both nonlinearity and a correlation between process noise and measurement output, the following derivation is developed. This derivation is inspired by the EKF formulation presented in [22] and the Kalman Filter derivations in [23] . Additionally, the presence of process noise in the measurement equation shares similarities with the case where $w[n]$ and $v[n]$ are correlated, as discussed in [24]. Therefore, aspects of its derivation process have also been incorporated into this work.

Prediction Step:

The Kalman Filter is a recursive algorithm that consists of two distinctive steps, predictor and corrector. In the predictor step, given an initial estimate of the state, $\hat{x}[0] \sim \mathcal{N}(x_0, P_0)$, an estimation of state for one step in future, $(n+1)$, is calculated using observation information up to instant n, $Y^n = \{y[1], \ldots, y[n]\}$.

$$\begin{aligned} \hat{x}[n+1 \mid n] &= \mathbb{E}[x[n+1] \mid Y^n] \\ &= \mathbb{E}[\tilde{f}(x[n], u[n]) + \tilde{G}w[n] \mid Y^n] \\ &= \mathbb{E}[\tilde{f}(x[n], u[n]) \mid Y^n] + \tilde{G}\mathbb{E}[w[n] \mid Y^n] \end{aligned} \tag{26}$$

Expanding the $\tilde{f}(.)$ function in Taylor series about $\hat{x}[n \mid n]$, we get:

$$\tilde{f}(x[n], u[n]) \equiv \tilde{f}(\hat{x}[n \mid n], u[n]) + A(x[n] - \hat{x}[n \mid n]) + H.O.T. \tag{27}$$

where;

$$A = \left.\frac{\partial \tilde{f}}{\partial x}\right|_{\hat{x}[n|n]} \tag{28}$$

is the Jacobian of the function $\tilde{f}(.)$, and the higher order terms (H.O.T.) are considered negligible. Hence, the EKF is also known as the First-Order Filter [22]. Thus the expected value of $\tilde{f}(x[n], u[n])$ given Y^n is approximately:

$$\mathbb{E}[\tilde{f}(x[n], u[n]) \mid Y^n] \approx \tilde{f}(\hat{x}[n \mid n], u[n]) + A\mathbb{E}[e[n] \mid Y^n], \tag{29}$$

where the estimation error $e[n]$ is defined as:

$$e[n] = (x[n] - \hat{x}[n \mid n]), \tag{30}$$

and due to the unbiasedness condition for the EKF:

$$\mathbb{E}[e[n] \mid Y^n] = 0. \tag{31}$$

The second term of the equation (26) is no longer zero, unlike the conventional EKF, due to the direct correlation between process noise and measurement in our system model. To find the estimation of the process noise, the following equation is used [24]:

$$\mathbb{E}[w[n] \mid Y^n] = \bar{w}[n] + P_{WY} P_Y^{-1} Y_e[n], \tag{32}$$

where, $\bar{w}[n]$ indicates the mean value for $w[n]$ which is already defined to be zero. Y_e is the measurement error defined as:

$$Y_e[n] = y[n] - \tilde{h}(\hat{x}[n \mid n-1], u[n]). \tag{33}$$

The cross-covariance of process noise and measurement equation is given as:

$$P_{WY} = \mathbb{E}[(w[n])(Y_e[n])^T]. \tag{34}$$

Similar to equation (27), the $\tilde{h}(.)$ function is expanded using Taylor series around $\hat{x}[n \mid n]$:

$$\tilde{h}(x[n], u[n]) \equiv \tilde{h}(\hat{x}[x \mid x], u[n]) + C\big(x[n] - \hat{x}[n \mid n]\big) + H.O.T. \tag{35}$$

where;

$$C = \left.\frac{\partial \tilde{h}}{\partial x}\right|_{\hat{x}[n|n]} \tag{36}$$

Again, since EKF is a first order filter, the higher order terms are neglected. Hence the measurement error $Y_e[n]$ is expressed as:

$$\begin{gathered} Y_e[n] = \tilde{h}(\hat{x}[x \mid x], u[n]) + C\big(x[n] - \hat{x}[n \mid n]\big) + \tilde{H}[n]w[n] + v[n] - \tilde{h}(\hat{x}[x \mid x], u[n]) - C\big(\hat{x}[n \mid n-1] - \hat{x}[n \mid n]\big) \\ Y_e[n] = C\big(x[n] - \hat{x}[n \mid n-1]\big) + \tilde{H}[n]w[n] + v[n]. \end{gathered} \tag{37}$$

Plugging equation (37) back into equation (34), results in:

$$P_{WY} = \mathbb{E}[(w[n])(C(x[n] - \hat{x}[n \mid n-1]) + \tilde{H}[n]w[n] + v[n])^T].$$

Considering the assumptions of (25) and the fact that the prediction error $(x[n] - \hat{x}[n \mid n-1])$ is not correlated with $w[n]$, we get:

$$P_{WY} = \tilde{H}[n]Q^T. \tag{38}$$

Similarly, the covariance of the measurement error, denoted as P_Y is derived as follows:

$$\begin{gathered} P_Y = \mathbb{E}[(Y_e[n])(Y_e[n])^T] \\ = \mathbb{E}\big[\big(C\big(x[n] - \hat{x}[n \mid n-1]\big) + \tilde{H}[n]w[n] + v[n]\big).\big(C\big(x[n] - \hat{x}[n \mid n-1]\big) + \tilde{H}[n]w[n] + v[n]\big)^T\big] \end{gathered}$$

After some manipulations, it reduces to:

$$P_Y = CP[n \mid n-1]C^T + \tilde{H}[n]Q\tilde{H}[n]^T + R. \tag{39}$$

Plugging equation (38) and (39) into (32) results in:

$$\hat{w}[n] = \tilde{H}[n]Q^T(CP[n \mid n-1]C^T + \tilde{H}[n]Q\tilde{H}[n]^T + R)^{-1}Y_e[n]. \tag{40}$$

Finally, the estimated $\hat{x}[n+1 \mid n]$ is obtained by plugging (29) and (40) into (26),

$$\hat{x}[n+1 \mid n] = \tilde{f}(\hat{x}[n \mid n], u[n]) + \tilde{G}\tilde{H}Q^T(CP[n \mid n-1]C^T + \tilde{H}[n]Q\tilde{H}[n]^T + R)^{-1}Y_e[n]. \tag{41}$$

Update Step:

In this step, we have the prediction of the state estimate $\hat{x}[n \mid n-1]$ and the new measurement $y[n]$ in hand. The updated estimate of the state, defined as $\hat{x}[n \mid n]$, is basically the weighted summation of these two terms.

$$\hat{x}[n \mid n] = \hat{x}[n \mid n-1] + K[n]Y_e[n], \tag{42}$$

where $K[n]$ is defined as the correction gain.

Then plugging the measurement error $Y_e[n]$ from equation (37), we get:

$$\begin{aligned} \hat{x}[n \mid n] &= \hat{x}[n \mid n-1] + K[n]\big(C(x[n] - \hat{x}[n \mid n-1]) + \tilde{H}[n]w[n] + v[n]\big) \\ &= (I - K[n]C)\hat{x}[n \mid n-1] + K[n]Cx[n] + K[n]\tilde{H}[n]w[n] + K[n]v[n]. \end{aligned} \tag{43}$$

The estimation error $e[n]$ is defined as:

$$\begin{aligned} e[n] &= x[n] - \hat{x}[n \mid n] \\ &= (I - K[n]C)(x[n] - \hat{x}[n \mid n-1]) - K[n]\tilde{H}[n]w[n] - K[n]v[n]. \end{aligned} \tag{44}$$

Accordingly, the error covariance matrix for the updated estimate can be found by:

$$\begin{aligned} P[n \mid n] &= \mathbb{E}\big[e[n]e[n]^T\big] \\ &= \mathbb{E}\big[((I - K[n]C)(x[n] - \hat{x}[n \mid n-1]) - K[n]\tilde{H}[n]w[n] - K[n]v[n]). \\ &\quad ((I - K[n]C)(x[n] - \hat{x}[n \mid n-1]) - K[n]\tilde{H}[n]w[n] - K[n]v[n])^T\big] \end{aligned} \tag{45}$$

Since the prior estimation error $(x[n] - \hat{x}[n \mid n-1])$, process noise $w[n]$, and measurement noise $v[n]$ are uncorrelated, this simplifies to:

$$P[n \mid n] = (I - K[n]C)P[n \mid n-1](I - K[n]C)^T + K[n]\tilde{H}[n]Q\tilde{H}[n]^TK[n]^T + K[n]RK[n]^T. \tag{46}$$

Now the goal is to find the correction gain in such a way that it minimizes the update error covariance matrix $P[n \mid n]$. Since the trace of the $P[n \mid n]$ is essentially the sum of mean square errors, and it is a convex function of the gain, $K[n]$, taking the derivative of it w.r.t correction gain and setting it to zero results in the optimal gain.

$$\frac{d}{dK[n]}\mathrm{Tr}(P[n|n]) = 0. \tag{47}$$

The trace of the update error covariance is:

$$\begin{aligned} \mathrm{Tr}(P[n \mid n]) = \mathrm{Tr}(P[n \mid n-1]) - 2\mathrm{Tr}(CK[n]P[n \mid n-1]) + \mathrm{Tr}(K[n]CP[n \mid n-1]C^TK[n]^T) + \\ \mathrm{Tr}(K[n]\tilde{H}[n]Q\tilde{H}[n]^TK[n]^T) + \mathrm{Tr}(K[n]RK[n]^T). \end{aligned} \tag{48}$$

Then, taking the derivative with respect to $K[n]$ will lead to:

$$K[n] = P[n|n-1]C^T(CP[n|n-1]C^T + \tilde{H}[n]Q\tilde{H}[n]^T + R)^{-1}. \tag{49}$$

Substituting equation (49) into Equations (42) and (46) and performing the necessary mathematical manipulations, gives:

$$\hat{x}[n \mid n] = \hat{x}[n \mid n-1] + P[n \mid n-1]C^T(CP[n|n-1]C^T + \tilde{H}[n]Q\tilde{H}[n]^T + R)^{-1}Y_e[n]. \tag{50}$$

$$P[n \mid n] = P[n \mid n-1] - P[n|n-1]C^T(CP[n|n-1]C^T + \tilde{H}[n]Q\tilde{H}[n]^T + R)^{-1}CP[n \mid n-1] \tag{51}$$

To complete the recursion, we compute the covariance of the prediction estimate as follows:

$$P[n+1 \mid n] = \mathbb{E}[\big(x[n+1] - \hat{x}[n+1|n]\big).\big(x[n+1] - \hat{x}[n+1|n]\big)^T]. \tag{52}$$

Using the linearization of the nonlinear function $\tilde{f}(.)$ as given in equation (28), we can write the prediction error as follows:

$$\begin{aligned} e[n+1|n] &= x[n+1] - \hat{x}[n+1|n] \\ &= \tilde{f}(x[n], u[n]) + \tilde{G}w[n] - \tilde{f}(\hat{x}[n \mid n], u[n]) - \tilde{G}\tilde{H}[n]Q^T(P_Y)^{-1}Y_e[n] \\ &= A(x[n] - \hat{x}[n|n]) + \tilde{G}w[n] - \tilde{G}\tilde{H}[n]Q^T(P_Y)^{-1}Y_e[n]. \end{aligned} \tag{53}$$

Substituting equation (50) into (53), gives:

$$\begin{aligned} e[n+1 \mid n] = A\big((I - K[n]C)(x[n] - \hat{x}[n \mid n-1]) - K[n]\tilde{H}[n]w[n] - K[n]v[n]\big) + \tilde{G}w[n] \\ -\tilde{G}\tilde{H}[n]Q^TP_Y^{-1}\big(C\big(x[n] - \hat{x}[n \mid n-1]\big) + \tilde{H}[n]w[n] + v[n]\big) \\ = \big(A(I - K[n]C) - \tilde{G}\tilde{H}[n]Q^TP_Y^{-1}C\big)(x[n] - \hat{x}[n \mid n-1]) \\ -\big(AK[n]\tilde{H}[n] + \tilde{G}\tilde{H}[n]Q^TP_Y^{-1}\tilde{H}[n] - \tilde{G}\big)w[n] \\ -\big(AK[n] + \tilde{G}\tilde{H}[n]Q^TP_Y^{-1}\big)v[n] \end{aligned} \tag{54}$$

Plugging back equation (54) into (52) results in:

$$\begin{aligned} P[n+1 \mid n] = \mathbb{E}[(e[n+1 \mid n]).(e[n+1 \mid n])^T] \\ = A(I - K[n]C)P[n \mid n-1](A(I - K[n]C))^T - (AK[n]\tilde{H}[n])Q(AK[n]\tilde{H}[n])^T \\ -(AK[n])R(AK[n])^T + \tilde{G}Q\tilde{G}^T - (\tilde{G}\tilde{H}[n]Q^TP_Y^{-1}C)P[n \mid n-1](\tilde{G}\tilde{H}[n]Q^TP_Y^{-1}C)^T \\ -(\tilde{G}\tilde{H}[n]Q^TP_Y^{-1}\tilde{H}[n])Q(\tilde{G}\tilde{H}[n]Q^TP_Y^{-1}\tilde{H}[n])^T - (\tilde{G}\tilde{H}[n]Q^TP_Y^{-1})R(\tilde{G}\tilde{H}[n]Q^TP_Y^{-1})^T \\ = AP[n \mid n]A^T + \tilde{G}Q\tilde{G}^T - (\tilde{G}\tilde{H}Q^TP_Y^{-1})\big(CP[n \mid n-1]C^T + \tilde{H}[n]Q\tilde{H} + R\big)(\tilde{G}\tilde{H}[n]Q^TP_Y^{-1})^T \\ = AP[n \mid n]A^T + \tilde{G}Q\tilde{G}^T - \tilde{G}\tilde{H}[n]Q^TP_Y^{-1}Q\tilde{H}[n]^T\tilde{G}^T \end{aligned} \tag{55}$$

3.2.2 Summary of the Derived EKF

Finally, the summary of the obtained EKF is brought as follows:

- Prediction step:

$$\hat{x}[n+1 \mid n] = \tilde{f}(\hat{x}[n \mid n], u[n]) + \tilde{G}\tilde{H}[n]Q^TP_Y^{-1}Y_e[n]. \tag{56}$$

$$P[n+1 \mid n] = AP[n \mid n]A^T + \tilde{G}Q\tilde{G}^T - \tilde{G}\tilde{H}[n]Q^TP_Y^{-1}Q\tilde{H}[n]^T\tilde{G}^T \tag{57}$$

- Update step:

$$\hat{x}[n \mid n] = \hat{x}[n \mid n-1] + P[n \mid n-1]C^TP_Y^{-1}Y_e[n]. \tag{58}$$

$$P[n \mid n] = \big(I - P[n|n-1]C^TP_Y^{-1}C\big)P[n \mid n-1] \tag{59}$$

3.3 Real-Time PPF Control Adaptation with EKF Estimator

In this section, the control loop is completed by integrating the EKF to estimate the system's resonance frequency in real time and recursively update the parameters of the H_2-optimized PPF controller. Assuming that the initial state estimate is sufficiently close to the true state, the EKF equations (56-59), as derived in the previous section, propagate the estimate of the augmented state at each sampling time T_s. The estimated stiffness is then used to determine the estimated resonance frequency $\hat{\omega}_n$ of the plant, using equation (12), which serves as the reference for the controller's parameter adaptation.

Next, utilizing equations (8-10), the PPF controller parameters, consisting of the filter's natural frequency ω_c, damping ratio ζ_c, and gain k, are updated using $\hat{\omega}_n$ and a predefined static open-loop gain, g. Finally, the PPF controller outputs the optimal control input, u, which is applied to the plant, resulting in continuous suppression of resonance frequencies.

Figure 3 demonstrates a high-level block diagram of the proposed control system.

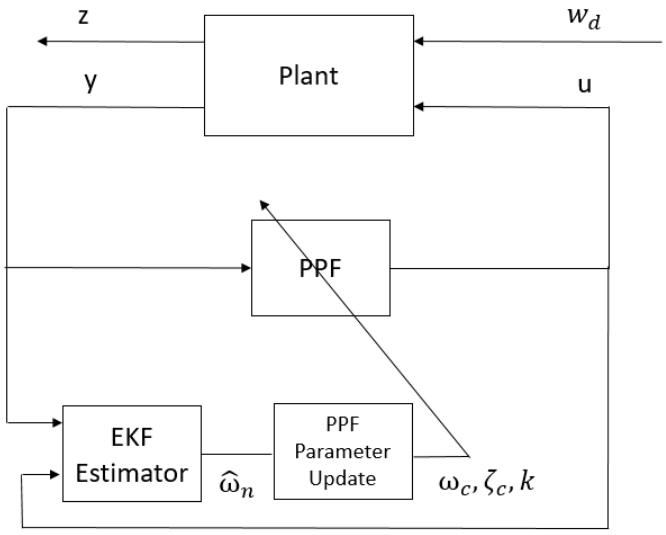

Figure 3: Block diagram of the adaptive PPF controller.

3.4 Stability and Robustness analysis

In this section, the stability analysis of the closed-loop system, consisting of the plant and the PPF controller, is conducted [16]. The closed-loop system model is governed by the following equation, which incorporates equation (9) representing the plant and equation (14) describing the PPF controller model.

$$\begin{bmatrix} \ddot{x} \\ \ddot{q} \end{bmatrix} + \begin{bmatrix} \frac{c}{m} & 0 \\ 0 & 2\zeta\omega_c \end{bmatrix} \begin{bmatrix} \dot{x} \\ \dot{q} \end{bmatrix} + \begin{bmatrix} \omega_n^2 & -\omega_c b_u k_a \\ -\omega_c f_y k_s & \omega_c^2(1 - k_s d_{yu} k_a) \end{bmatrix} \begin{bmatrix} x \\ q \end{bmatrix} = \begin{bmatrix} b_w \\ d_{yw} k_s \omega_c \end{bmatrix} w, \tag{60}$$

$$z = \begin{bmatrix} f_z & d_{zu} k_a \omega_c \end{bmatrix} \begin{bmatrix} x \\ q \end{bmatrix} + d_{zw} w. \tag{61}$$

The system remains stable if the mass, damping, and stiffness matrices are symmetric and positive (semi-) definite. The mass matrix is a 2×2 identity matrix, which is inherently symmetric and positive definite. Similarly, the damping matrix is symmetric and remains positive definite if $\frac{c}{m} > 0$ and $2\zeta\omega_c > 0$. These conditions hold true due to physical constraints, mass and damping coefficients are inherently positive, and because the control parameters are restricted to positive values. Finally, the stiffness matrix is symmetric if:

$$b_u k_a = f_y k_s. \tag{62}$$

This condition holds by choosing appropriate k_s and k_a.

Additionally, we argue that the stiffness matrix is also positive definite if the following condition applies.

$$\begin{bmatrix} \omega_n^2 & -\omega_c b_u k_a \\ -\omega_c f_y k_s & \omega_c^2(1 - k_s d_{yu} k_a) \end{bmatrix} \succ 0 \tag{63}$$

Using a Schur complement, it can equivalently be written as:

$$\omega_n^2 > 0 \tag{64}$$

$$\begin{aligned} \omega_c^2(1 - k_s d_{yu} k_a) - (\omega_c f_y k_s)(\frac{1}{\omega_n^2})(\omega_c b_u k_a) > 0 \\ \omega_c^2(1 - k_s k_a(d_{yu} + \frac{f_u b_u}{\omega_n^2})) > 0 \end{aligned} \tag{65}$$

To satisfy condition (65), the term inside the parentheses is selected to ensure a positive value. In other words, the static open-loop gain, g, defined as:

$$g = k_s k_a(d_{yu} + \frac{f_u b_u}{\omega_n^2}), \tag{66}$$

should be chosen within the range $0 < g < 1$. Ensuring that all these conditions hold guarantees the closed-loop stability of the system. However, this may raise the question of how to appropriately select g ! As discussed in Chapter 2 and more in depth in [16], the PPF controller is optimized with respect to its parameters while treating g as a free tuning parameter. The selection of g directly influences robustness and required actuation power. For instance, a smaller g leads to a larger gain margin in the Nyquist plot, enhancing robustness. However, this also results in an increased H_2 norm, which implies weaker performance in resonance suppression. Additionally, reducing g necessitates higher actuation input power, as explicitly demonstrated in [16]. Finally, the choice of g represents a trade-off between robustness, performance, and actuation power requirements. The appropriate value should be selected based on the specific priorities and constraints of the system. Once a proper value for g is selected, PPF parameters can be obtained using equations (8), (9), and (10).

Unlike the standard KF, the convergence of the EKF cannot be guaranteed in general. As previously mentioned, the EKF operates by linearizing the system dynamics around the estimated trajectory. Consequently, if the system shows strong nonlinearities, even small estimation errors can lead to significant deviations during the linearization process, potentially causing the estimation to diverge from the true state.

In our case, the system dynamics are bilinear, and the stiffness parameter is assumed to evolve at a rate that allows the EKF to effectively track it in practice. Bilinear systems, while still nonlinear, tend to show more favorable filtering properties compared to fully nonlinear systems, as their structure often permits a more controlled error propagation. However, the presence of a nonlinear measurement equation introduces an additional source of complexity, as linearization errors in the measurement update step may further affect the filter's robustness.

One key factor affecting the robustness of the EKF is its sensitivity to inaccurate state initialization. Compared to the standard KF, the EKF is more prone to divergence if the initial state estimate is far from the true state, as poor initialization can lead to incorrect linearization points [21]. This sensitivity is particularly problematic in nonlinear systems, where the filter's ability to recover from poor initial conditions is limited. As it will be discussed later, methods such as adaptive covariance tuning [25], robust filtering techniques [26], or iterated EKF approaches [27] could be considered to tackle this problem.

Despite these theoretical challenges, the approach remains effective in our case, as demonstrated by the results. The specific characteristics of the bilinear system and the relatively slow-varying stiffness parameter contribute to the EKF's ability to maintain stable and accurate state estimation within practical limits.

4 Simulations

4.1 Simulation Setup

Plant Parameters

In this section, the performance of the proposed controller from the last chapter, demonstrated in Figure 3, is evaluated through numerical simulations. As previously introduced in Chapter 2 and shown in Figure 1, the considered plant is a cantilever beam, modeled as a single degree of freedom system. The governing mathematical equations for this system is given in equations (1) and (2).

The parameters used for the simulations are presented in Table 1. These parameters were selected to accurately reflect the dynamic behavior of the beam, particularly its first resonance mode of T_{zw}, which is the target for suppression by the adaptive PPF controller.

Table 1: Cantilever Beam System Parameters

Parameter	Symbol	Value
Equivalent Mass	m	1 kg
Equivalent Stiffness	$k(t)$	[100,300] N/m
Equivalent Damping	c	0.001 Ns/m
Input Matrix	$\begin{bmatrix} B_u & B_d \end{bmatrix}$	$\begin{bmatrix} 10 & 80 \end{bmatrix}$
Output Matrix	$\begin{bmatrix} f_z & f_y \end{bmatrix}$	$\begin{bmatrix} 1 & 1 \end{bmatrix}$
System Parameters	$\begin{bmatrix} \gamma_{yu} & \gamma_{yw} \\ \gamma_{zu} & \gamma_{zw} \end{bmatrix}$	$\begin{bmatrix} 3.2774 & -1 \\ 0 & -0.1708 \end{bmatrix}$

Simulation Framework

To validate the effectiveness of the adaptive PPF controller, the system is simulated under realistic excitation conditions. The beam is excited by an external disturbance, w_d, which originates from ground vibrations. The system response is observed at the beam's tip. The control input, u, is applied through a piezoelectric actuator mounted on the beam, and a piezoelectric sensor is used to measure the displacements corresponding to the same degree of freedom as the actuator.

The closed-loop simulation setup follows the block diagram in Figure 3. At each time step (T_s), the EKF estimates the system's stiffness parameter, which is used to update the resonance frequency $\hat{\omega}_n$. The updated frequency is then used to adaptively tune the PPF controller parameters in real time, ensuring robust suppression of resonance vibrations. Table 2 gives numerical values chosen for Simulation.

Table 2: Simulation Parameters

Parameter	Symbol	Value
Ground disturbance	$w_d(t)$	White noise, $\mathcal{N}(0, 0.01^2)$
Measurement noise	$v(t)$	White noise, $\mathcal{N}(0, 0.01^2)$
Sampling time	T_s	0.001 s
Static open-loop gain	g	0.1

4.2 Performance Evaluation of the EKF Estimator

In this section, the effectiveness of the EKF estimator in tracking the time-varying stiffness of the plant is analyzed in an open-loop configuration. It is shown that due to the elasto-kinematic effect [19], the stiffness of flexures in their support direction decreases under large deflections. While previous studies [28] indicate that this variation exhibits a nonlinear behavior, for simplicity, a constant rate of stiffness change is assumed in this study.

Being inspired by [10], where it is demonstrated that the resonance frequency in real applications can double over the course of the deflection process, a constant rate of change is chosen. Specifically, in this setup, the stiffness is assumed to vary at a rate that leads to a doubling of the resonance frequency within a 40-second operational period.

Achieving accurate estimation with the EKF relies on several key factors, including appropriately tuned measurement and process noise covariances (R and Q) and a sufficiently excitating signal. In the following subsections, the influence of these factors on the estimation accuracy is systematically analyzed.

Tuning Q and R

To achieve an accurate estimation of the stiffness, careful tuning of the process and measurement noise covariances is required. The measurement noise covariance is relatively straightforward to determine. In this simulation, the measurement noise is modeled as zero-mean white noise with a standard deviation of 0.01, resulting in a covariance value of $R = 10^{-4}$. Notably, even in experimental scenarios, the measurement noise covariance can be directly determined, as the noise characteristics of the measurement signal can be extracted from the sensor data.

On the other hand, tuning the process noise covariance requires more consideration. The process noise covariance matrix Q is defined as a diagonal 2×2 matrix, where one element corresponds to the disturbance noise affecting the velocity state, and the other accounts for the unknown stiffness dynamics:

$$Q = \begin{bmatrix} Q_d & 0 \\ 0 & Q_k \end{bmatrix}$$

The disturbance noise w_d is modeled as zero-mean white noise with a standard deviation of 0.01, leading to $Q_d = 10^{-4}$, similar to R. However, tuning Q_k requires additional attention. Since the stiffness variation is generally unknown and is assumed to follow a constant rate in the state-space model, selecting an appropriate value for Q_k is crucial. The value of Q_k should be large enough for the estimator to attribute output prediction errors more to stiffness inaccuracies than to measurement noise or w_d.

Figure 4 illustrates the impact of tuning Q_k on stiffness estimation. It is evident that increasing Q_k enhances the filter's ability to track stiffness variations. However, increasing Q_k indefinitely does not lead to perfect estimation. A high Q_k results in an overly aggressive estimator, introducing fluctuations around the correct stiffness value. As shown in Figure 4, larger values of Q_k lead to noisier and less smooth estimates. Furthermore, as discussed later, excessive fluctuations in estimated stiffness can degrade controller performance and negatively impact vibration suppression. Therefore, tuning the estimator involves a bias-variance trade-off that must be carefully managed.

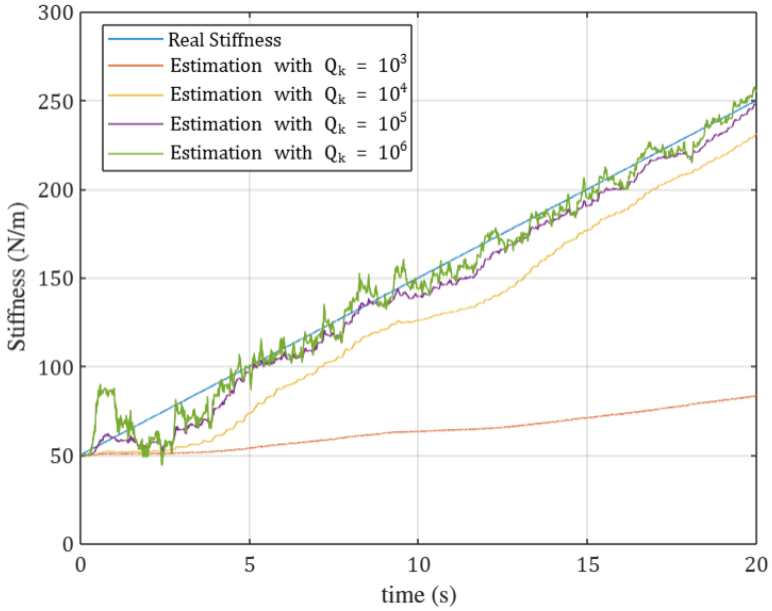

Figure 4: Influence of tuning Q_k on better estimation.

Additionally, it can be observed that for larger stiffness variations, higher values of Q_k are required. As the rate of stiffness change increases, the estimator must allow for more significant variations at each time step, necessitating a larger covariance value to account for this effect. Figure 5 illustrates this phenomenon: with a fixed $Q_k = 10^5$, the estimation accuracy deteriorates as the stiffness variation rate increases. For better demonstration, the mean stiffness estimation error over the simulation period is calculated for each case. The results show that as the stiffness variation rate increases, estimation errors become more significant, emphasizing the importance of properly tuning Q_k for different operating conditions.

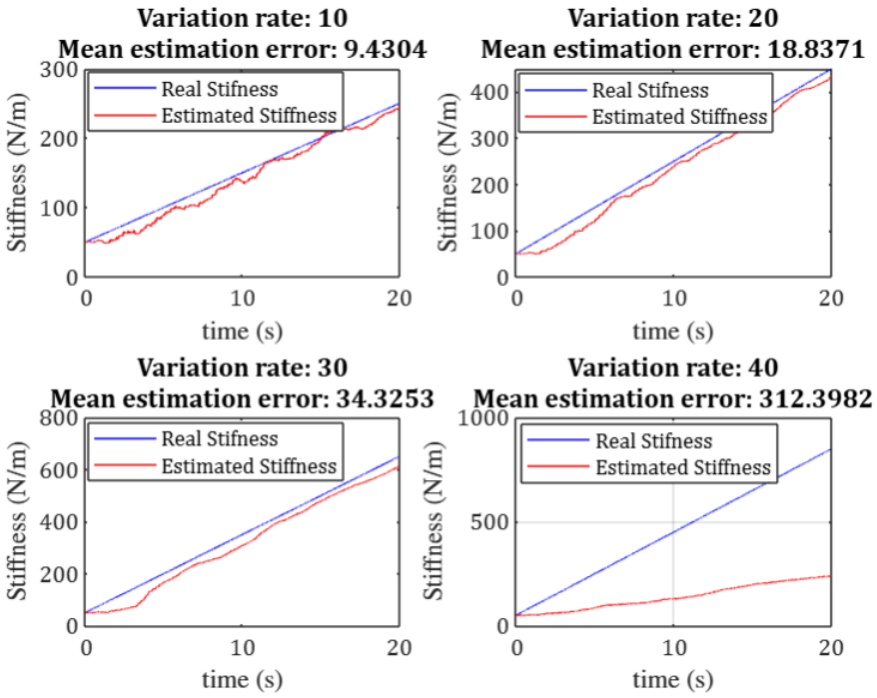

Figure 5: Effect of stiffness variation rate on estimation accuracy for a constant Q_k.

4.3 Performance Evaluation of Fixed-Parameter PPF Controller

In this section, the performance of the PPF controller with fixed parameters is assessed under varying resonance frequencies. This analysis will later highlight the necessity of adapting PPF parameters, which is the core objective of this thesis.

To conduct this evaluation, it is assumed that the average stiffness value over the variation period is known and is used to compute the PPF parameters using equations (8-10).

To quantify the suppression performance, two evaluation methods are employed. First, the H_2 norm of the open-loop and closed-loop frequency responses of T_{zw} is computed, and their ratio is used as a measure of resonance suppression effectiveness at each time instance when the stiffness turns to a new value.

The second evaluation method involves calculating the ratio between the H_∞ norm of the closed-loop system (T_{zw}) and its DC gain, referred to as the "Pseudo q factor." This terminology is inspired and arises from the fact that, for second-order systems, this ratio is commonly known as the "q factor." However, since the PPF controller increases the system order to four, the frequency response exhibits two close resonance peaks instead of a single one. The pseudo q factor considers the resonance peak with the highest magnitude. Although not a strict theoretical definition, this metric provides an intuitive measure of suppression effectiveness.

Figure 6 illustrates the H_2 norm ratio and the pseudo q factor. The results indicate that the best suppression performance occurs when the actual stiffness closely matches the assumed nominal value. As the deviation between real and assumed stiffness increases, the suppression effectiveness deteriorates.

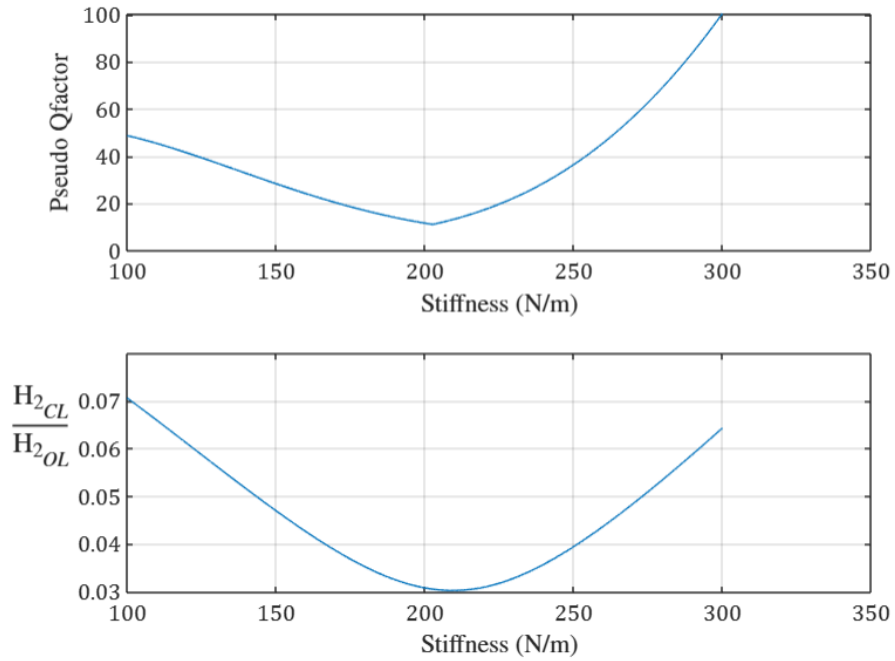

Figure 6: Pseudo q factor and H_2 norm ratio of the closed-loop and open-loop system for a fixed nominal stiffness of 200 N/m.

4.4 Performance Evaluation with Accurate Stiffness Knowledge

In this section, it is assumed that an accurate approximation of the real stiffness dynamics has been obtained through system identification. As expected, under these conditions, the PPF controller achieves optimal performance, adapting precisely to each resonance frequency variation throughout the workspace.

Figure 7 illustrates the optimal suppression performance using the previously defined evaluation metrics, demonstrating the effectiveness of the controller when exact stiffness values are available at each time instance.

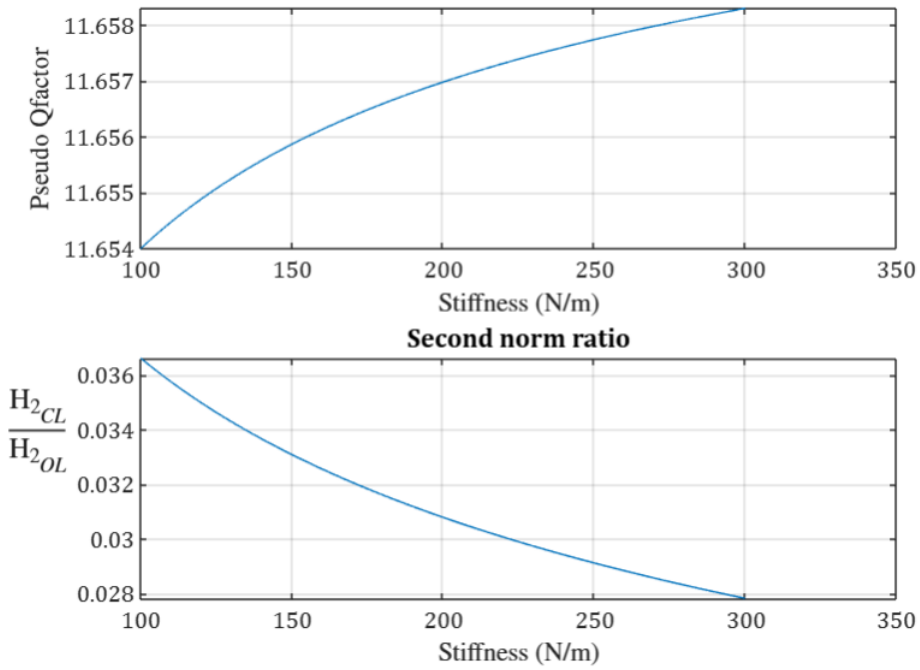

Figure 7: Pseudo q factor and H_2 norm ratio of the closed-loop and open-loop system (T_{zw}) for accurately known stiffness at each time instance.

4.5 Adaptive Optimal PPF Controller Based on EKF Observer

In this section, the resonance frequency of the system is estimated in real-time using the EKF, which subsequently updates the PPF parameters accordingly. For a stiffness variation with a slope of 5 over 40 seconds, Figure 8 demonstrates that the EKF effectively tracks the stiffness changes throughout the simulation. The measurement and process noise covariances are set to $R = 10^3$ and

$$Q = 10^3 \times \begin{bmatrix} 1 & 0 \\ 0 & 5 \times 10^5 \end{bmatrix}$$

respectively. It should be noted that R and Q are divided by the sampling time T_s to be properly incorporated into the discrete EKF algorithm.

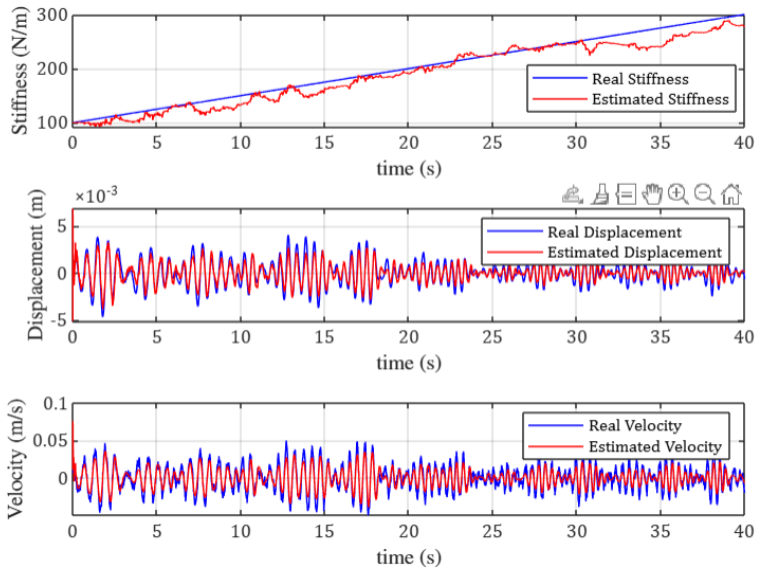

Figure 8: State estimation using EKF.

Figure 9 provides a closer examination of the stiffness estimation error. While noticeable fluctuations around the true stiffness value still remain, reducing Q_k would lead to a larger steady-state deviation from the actual stiffness, which is also undesirable. This highlights the trade-off in selecting an appropriate Q_k, balancing estimation accuracy and noise sensitivity.

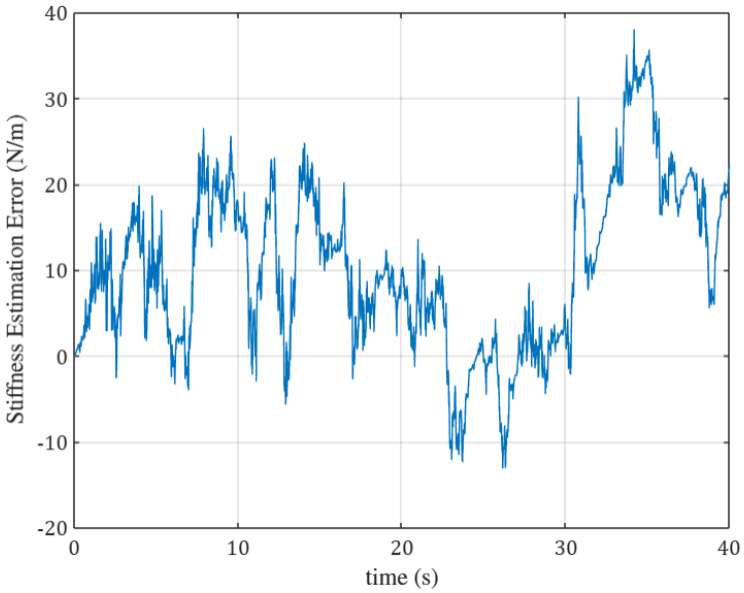

Figure 9: Stiffness estimation error.

Figures 10 and 11 illustrate the effectiveness of the proposed indirect adaptive PPF controller. Despite initial fluctuations at the beginning of the simulation, the controller can successfully attenuate

the resonance, demonstrating its capability in dealing with resonance frequency variations due to stiffness changes.

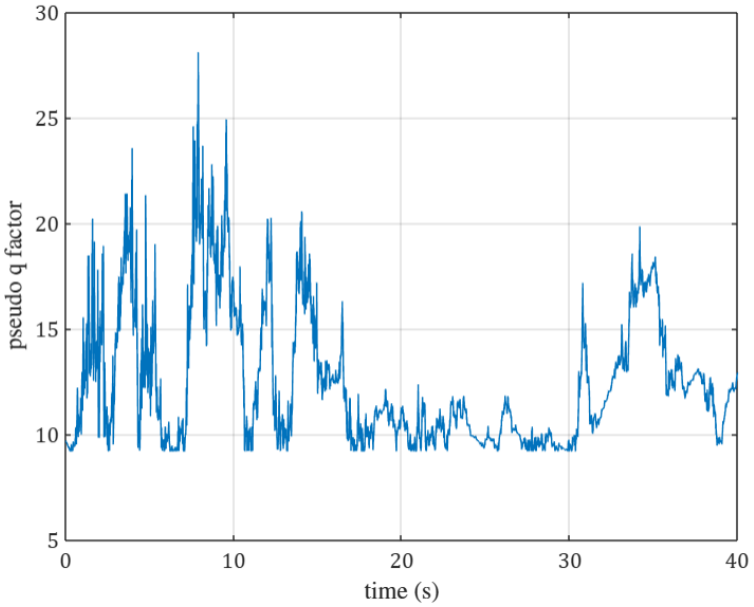

Figure 10: Performance of the adaptive PPF controller indicated by Pseudo q factor.

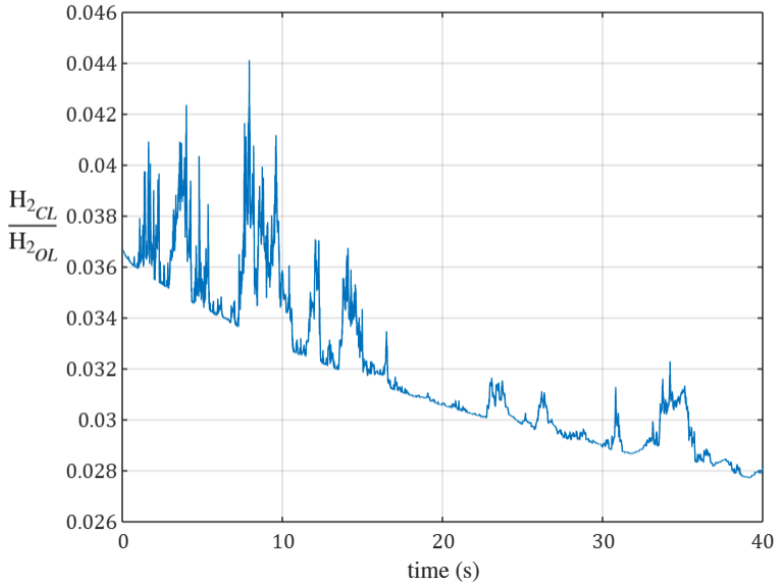

Figure 11: Performance of the adaptive PPF controller indicated by H_2 norm ratio of close-loop and open-loop system.

Moreover, a decreasing trend in Figure 11 is observed which is expected, as stiffer systems inherently exhibit lower resonance peaks. Consequently, as stiffness increases throughout the simulation, the H_2 norm of the system naturally decreases, independent of the controller's suppression effect.

A common observation from Figures 10 and 11 is the less robustness of the adaptive controller to the estimation inaccuracies at lower stiffness values, particularly at the beginning of the simulation. This behavior is further analyzed by examining the sensitivity of the adaptive PPF controller to errors in stiffness estimation. Figure 12 illustrates the variation of the pseudo Q-factor over a stiffness range of $[40, 140]$ under a fixed estimation deviation. The results indicate that the same estimation error has more effect at lower stiffness values.

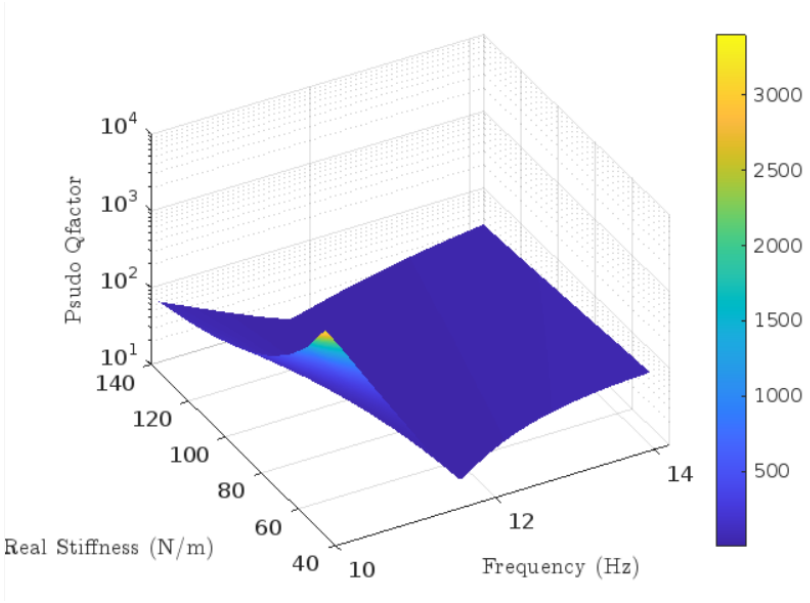

Figure 12: Sensitivity of the adaptive PPF controller to stiffness estimation errors.

4.6 Comparison of Different PPF Control Strategies

This section presents a comparison between the previously discussed control strategies: the fixed-parameter PPF controller, the PPF controller with foreknowledge of stiffness variations, and the proposed adaptive PPF controller. Figures 13 and 14 illustrate that the proposed adaptive controller closely follows the performance of the PPF controller with exact stiffness knowledge, whereas the fixed-parameter PPF controller exhibits weaker performance when the stiffness deviates from its assumed nominal value.

Furthermore, Figure 13 depicts the gain margin $(1 - g)$, computed using equation (66), for the three studied cases. It can be observed that both the adaptive PPF and the optimal PPF with stiffness foreknowledge maintain the predefined gain margin (as noted in Table 2). However, this is not the case for the fixed-parameter PPF controller. Notably, overestimating the stiffness leads to a reduction in the gain margin, which, as will be demonstrated in the following section, can also pose a risk of destabilizing the system.

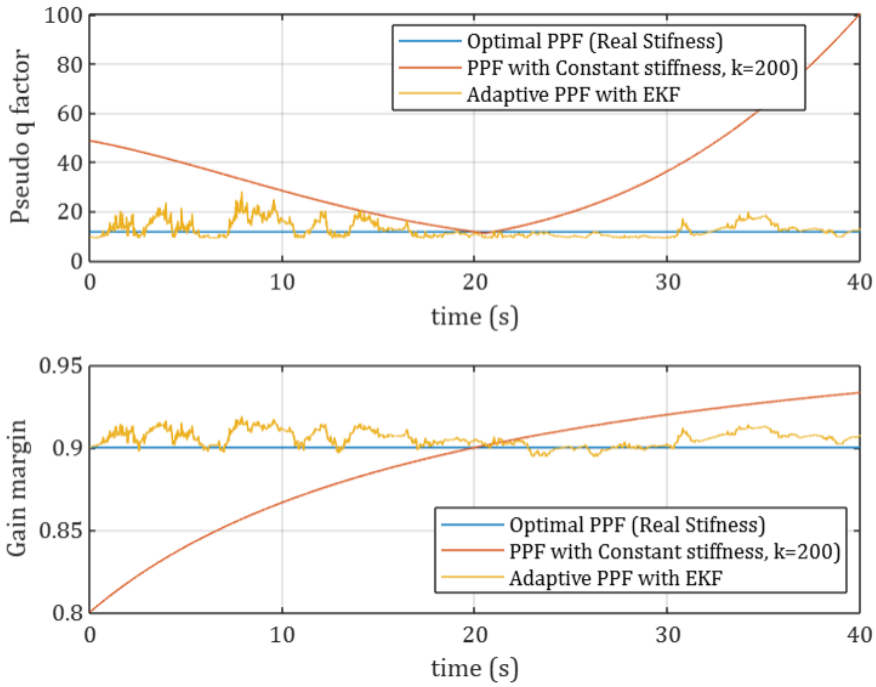

Figure 13: Performance comparison of gain margin and pseudo q factor for different discussed PPF controllers.

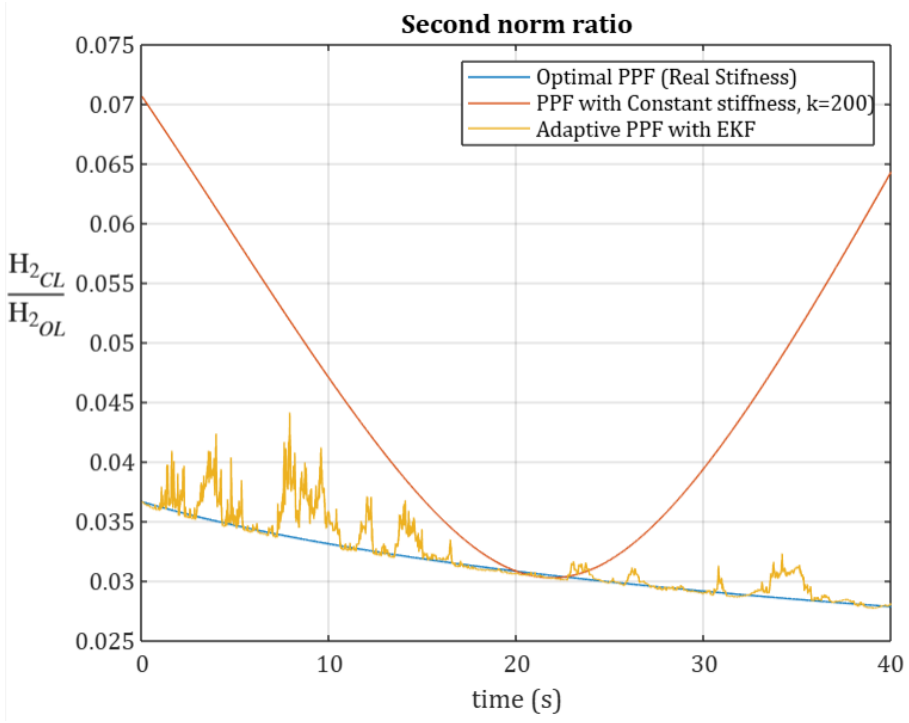

Figure 14: Performance comparison of the discussed PPF controller using their second norm ratio.

5 Conclusion and Future Recommendations

In this study, a PPF controller with an EKF-based resonance frequency estimator was developed. This controller is specifically designed to suppress parasitic resonance frequencies in a cantilever beam excited by ground vibrations while addressing the issue of varying resonance frequencies arising from stiffness changes due to large deflections and elasto-kinematic effects. The system model was reduced to a single-degree-of-freedom system to only capture the dominant low-frequency resonance. It was demonstrated that incorporating a feed-through term in the system model significantly improved the accuracy of the reduced-order SDoF representation, allowing it to fit the real system model adequately up to its second vibration mode.

Due to the presence of this feed-through term in the measurement equation, a modified joint EKF algorithm was required to handle the direct correlation between external disturbances and measurements. While the results of stiffness estimation using the derived EKF were promising, tuning the process covariance matrix proved to be a challenging and tedious task. Moreover, due to the nonlinearities of the system, the EKF may sometimes fail to converge to the correct stiffness values during the simulation.

Several potential directions for further research can be considered to improve the estimation accuracy and robustness. The first, and perhaps the most straightforward, is to identify the stiffness dynamics of the system beforehand and incorporate this information into the EKF equations. By doing so, large values for the stiffness covariance can be avoided, as a general trend for stiffness variations would already be known. Consequently, this approach would lead to smoother stiffness estimation with lower steady-state errors (bias), which is crucial for the proposed adaptive controller. A more accurate stiffness estimation would allow for more ambitious controller tuning, enabling higher static open-loop gain values and achieving even better resonance suppression while ensuring robustness throughout the simulation.

Another possible improvement involves utilizing adaptive covariance tuning, as discussed in [25]. As previously mentioned, achieving good EKF estimation requires carefully selecting the process (Q) and measurement (R) noise covariances. In this study, these covariances were kept constant throughout the entire simulation. However, in practical applications, measurement noise levels may vary due to several reasons such as payload changes, long-term fatigue effects, etc, all of which can change the system's state dynamics. By incorporating an adaptive covariance tuning algorithm within the EKF estimator, as proposed in [25], the estimator can dynamically adjust to these uncertainties, ensuring consistently reliable performance.

Additionally, the presented EKF estimator cannot be guaranteed to remain robust if the initial state estimate deviates significantly from the true state. In such situations, the EKF, essentially a first-order filter, may be linearized around an inaccurate state estimate, potentially leading to error accumulation and eventual divergence. This issue could be addressed using a robust Kalman filter, such as the method proposed in [26], where higher-order terms in the Taylor series expansion are not simply neglected but are instead treated as functions of state estimation errors and exogenous inputs with bounded H_∞ norms. This approach formulates the problem as a minimax estimation problem, which can be tackled using standard H_∞ techniques. While this method offers superior performance for highly nonlinear systems, its applicability should be evaluated in our case, as the system model exhibits bilinear properties, whereas the output measurement equation appears to introduce more significant nonlinearities.

The proposed adaptive PPF controller was shown to outperform the conventional fixed-parameter PPF controller, achieving performance comparable to that of a PPF controller with full foreknowledge of stiffness variations. The adaptive approach demonstrated improved robustness against uncertainties in stiffness variation while maintaining system stability across a wide range of operating conditions. However, as with other adaptive control strategies, this method is susceptible to the phenomenon of "bursting," where insufficient system excitation followed by an inaccurate parameter update results in large deviations from the correct estimation, leading to significant transient excitations. This issue can be mitigated by ensuring persistent excitation through exogenous input signals.

While the proposed adaptive PPF controller demonstrates promising results, further research could focus on refining its robustness and stability in the presence of uncertainties. Enhancing the estimation process through adaptive covariance tuning or robust filtering techniques could mitigate convergence issues and improve reliability. Future work could also explore real-time implementation and experimental validation to assess the controller's practical feasibility and performance in real-world applications.

References

[1] B. Babakhani, "Active damping of vibrations in high-precision motion systems," Ph.D. dissertation, University Library/University of Twente, ISBN: 9789036534642. DOI: 10.3990/1.9789036534642. [Online]. Available: http://dx.doi.org/10.3990/1.9789036534642.

[2] S. T. Smith, *Flexures: Elements of elastic mechanisms*, Aug. 2000. DOI: 10.1201/9781482282962. [Online]. Available: http://dx.doi.org/10.1201/9781482282962.

[3] M. Naves, R. Aarts, and D. Brouwer, "Large-stroke flexure hinges: Building-block-based spatial topology synthesis method for maximising flexure performance over their entire range of motion," English, *Mikroniek*, vol. 57, no. 3, pp. 5–9, 2017, ISSN: 0026-3699.

[4] C. D. Johnson, "Design of passive damping systems," *Journal of Vibration and Acoustics*, vol. 117, no. B, pp. 171–176, Jun. 1995, ISSN: 1528-8927. DOI: 10.1115/1.2838659. [Online]. Available: http://dx.doi.org/10.1115/1.2838659.

[5] M. Sahin and U. Aridogan, "Performance evaluation of piezoelectric sensor/actuator on active vibration control of a smart beam," *Proceedings of the Institution of Mechanical Engineers, Part I: Journal of Systems and Control Engineering*, vol. 225, no. 5, pp. 533–547, Jun. 2011, ISSN: 2041-3041. DOI: 10.1177/0959651811400974. [Online]. Available: http://dx.doi.org/10.1177/0959651811400974.

[6] A. Preumont, *Vibration Control of Active Structures*. Springer International Publishing, 2018, ISBN: 9783319722962. DOI: 10.1007/978-3-319-72296-2. [Online]. Available: http://dx.doi.org/10.1007/978-3-319-72296-2.

[7] C. Vasques and J. Dias Rodrigues, "Active vibration control of smart piezoelectric beams: Comparison of classical and optimal feedback control strategies," *Computers amp; Structures*, vol. 84, no. 22–23, pp. 1402–1414, Sep. 2006, ISSN: 0045-7949. DOI: 10.1016/j.compstruc.2006.01.026. [Online]. Available: http://dx.doi.org/10.1016/j.compstruc.2006.01.026.

[8] C. J. GOH and T. K. CAUGHEY, "On the stability problem caused by finite actuator dynamics in the collocated control of large space structures," *International Journal of Control*, vol. 41, no. 3, pp. 787–802, Mar. 1985, ISSN: 1366-5820. DOI: 10.1080/0020718508961163. [Online]. Available: http://dx.doi.org/10.1080/0020718508961163.

[9] L. Marinangeli, F. Alijani, and S. H. HosseinNia, "Fractional-order positive position feedback compensator for active vibration control of a smart composite plate," *Journal of Sound and Vibration*, vol. 412, pp. 1–16, Jan. 2018, ISSN: 0022-460X. DOI: 10.1016/j.jsv.2017.09.009. [Online]. Available: http://dx.doi.org/10.1016/j.jsv.2017.09.009.

[10] B. Seinhorst, M. Nijenhuis, and W. Hakvoort, "Feasibility of active material vibration suppression in a large stroke flexure hinge," *IFAC-PapersOnLine*, vol. 55, no. 27, pp. 166–171, 2022, ISSN: 2405-8963. DOI: 10.1016/j.ifacol.2022.10.506. [Online]. Available: http://dx.doi.org/10.1016/j.ifacol.2022.10.506.

[11] N. Nevaranta, S. Derammelaere, J. Parkkinen, *et al.*, "Online identification of a mechanical system in frequency domain using sliding dft," *IEEE Transactions on Industrial Electronics*, vol. 63, no. 9, pp. 5712–5723, Sep. 2016, ISSN: 1557-9948. DOI: 10.1109/tie.2016.2574303. [Online]. Available: http://dx.doi.org/10.1109/TIE.2016.2574303.

[12] J. Kang, S. Chen, and X. Di, "Online detection and suppression of mechanical resonance for servo system," in *2012 Third International Conference on Intelligent Control and Information Processing*, IEEE, Jul. 2012, pp. 16–21. DOI: 10.1109/icicip.2012.6391515. [Online]. Available: http://dx.doi.org/10.1109/ICICIP.2012.6391515.

[13] S. Nima Mahmoodi, M. Ahmadian, and D. J. Inman, "Adaptive modified positive position feedback for active vibration control of structures," *Journal of Intelligent Material Systems and Structures*, vol. 21, no. 6, pp. 571–580, Feb. 2010, ISSN: 1530-8138. DOI: 10.1177/1045389x10361631. [Online]. Available: http://dx.doi.org/10.1177/1045389X10361631.

[14] C. J. GOH and T. H. LEE, "Adaptive modal parameters identification for collocated position feedback vibration control," *International Journal of Control*, vol. 53, no. 3, pp. 597–617, Mar. 1991, ISSN: 1366-5820. DOI: 10.1080/00207179108953637. [Online]. Available: http://dx.doi.org/10.1080/00207179108953637.

[15] B. La Scala and R. Bitmead, "Design of an extended kalman filter frequency tracker," *IEEE Transactions on Signal Processing*, vol. 44, no. 3, pp. 739–742, Mar. 1996, ISSN: 1053-587X. DOI: 10.1109/78.489052. [Online]. Available: http://dx.doi.org/10.1109/78.489052.

[16] B. Seinhorst, M. Nijenhuis, and W. Hakvoort, "Gain margin constrained h2 and h∞ optimal positive position feedback control for piezoelectric vibration suppression," 2025. DOI: 10.2139/ssrn.5117631. [Online]. Available: http://dx.doi.org/10.2139/ssrn.5117631.

[17] H. Tjahyadi, F. He, and K. Sammut, "Vibration control of a cantilever beam using adaptive resonant control," vol. 3, Aug. 2004, 1776–1780 Vol.3, ISBN: 0-7803-8873-9. DOI: 10.1109/ASCC.2004.184902.

[18] G. Song, S. P. Schmidt, and B. N. Agrawal, "Experimental robustness study of positive position feedback control for active vibration suppression," *Journal of Guidance, Control, and Dynamics*, vol. 25, no. 1, 179a–1182, Jan. 2002, ISSN: 1533-3884. DOI: 10.2514/2.4865. [Online]. Available: http://dx.doi.org/10.2514/2.4865.

[19] S. Awtar, "Synthesis and analysis of parallel kinematic xy flexure mechanisms," 2003. [Online]. Available: https://api.semanticscholar.org/CorpusID:107212855.

[20] R. E. Kalman, "A new approach to linear filtering and prediction problems," *Journal of Basic Engineering*, vol. 82, no. 1, pp. 35–45, Mar. 1960, ISSN: 0021-9223. DOI: 10.1115/1.3662552. [Online]. Available: http://dx.doi.org/10.1115/1.3662552.

[21] T. Larsen, K. Hansen, N. Andersen, and O. Ravn, "Design of kalman filters for mobile robots; evaluation of the kinematic and odometric approach," in *Proceedings of the 1999 IEEE International Conference on Control Applications (Cat. No.99CH36328)*, ser. CCA-99, vol. 2, IEEE, pp. 1021–1026. DOI: 10.1109/cca.1999.801027. [Online]. Available: http://dx.doi.org/10.1109/CCA.1999.801027.

[22] G. Terejanu, "Extended kalman filter tutorial," 2009. [Online]. Available: https://api.semanticscholar.org/CorpusID:14331779.

[23] T. Lacey, "Tutorial: The kalman filter 11.1 introduction 11.2 mean squared error," 1998. [Online]. Available: https://api.semanticscholar.org/CorpusID:48574040.

[24] F. L. Lewis, L. Xie, and D. Popa, *Optimal and Robust Estimation: With an Introduction to Stochastic Control Theory*. CRC Press, Dec. 2017, ISBN: 9781315221656. DOI: 10.1201/9781315221656. [Online]. Available: http://dx.doi.org/10.1201/9781315221656.

[25] S. Akhlaghi, N. Zhou, and Z. Huang, "Adaptive adjustment of noise covariance in kalman filter for dynamic state estimation," in *2017 IEEE Power amp; Energy Society General Meeting*, IEEE, Jul. 2017, pp. 1–5. DOI: 10.1109/pesgm.2017.8273755. [Online]. Available: http://dx.doi.org/10.1109/PESGM.2017.8273755.

[26] G. Einicke and L. White, "Robust extended kalman filtering," *IEEE Transactions on Signal Processing*, vol. 47, no. 9, pp. 2596–2599, 1999, ISSN: 1053-587X. DOI: 10.1109/78.782219. [Online]. Available: http://dx.doi.org/10.1109/78.782219.

[27] J. Havlík and O. Straka, "Performance evaluation of iterated extended kalman filter with variable step-length," *Journal of Physics: Conference Series*, vol. 659, p. 012 022, Nov. 2015, ISSN: 1742-6596. DOI: 10.1088/1742-6596/659/1/012022. [Online]. Available: http://dx.doi.org/10.1088/1742-6596/659/1/012022.

[28] M. Nijenhuis, J. Meijaard, and D. Brouwer, "A 3-d nonlinear analytical stiffness model for deflected leaf springs," English, 33rd ASPE Annual Meeting 2018, ASPE 2018 ; Conference date: 04-11-2018 Through 09-11-2018, Nov. 2018, p. 517.